

Article

# Ab Initio Characterization of Magnetoelectric Coupling in Fe/BaTiO<sub>3</sub>, Fe/SrTiO<sub>3</sub>, Co/BaTiO<sub>3</sub> and Co/SrTiO<sub>3</sub> Heterostructures

Irina Piyanzina <sup>1,2,\*</sup> , Kirill Evseev <sup>1</sup> , Andrey Kamashev <sup>1</sup>  and Rinat Mamin <sup>1,2</sup>

<sup>1</sup> FRC Kazan Scientific Center of RAS, Zavoisky Physical-Technical Institute, 420029 Kazan, Russia; ekv97@mail.ru (K.E.); kamandi@mail.ru (A.K.); rf\_mamin@yahoo.com (R.M.)

<sup>2</sup> Institute of Physics, Kazan Federal University, 420008 Kazan, Russia

\* Correspondence: i.piyanzina@gmail.com

**Abstract:** Magneto-electric coupling is a desirable property for a material used in modern electronic devices to possess due to the favorable possibilities of tuning the electronic properties using a magnetic field and vice versa. However, such materials are rare in nature. That is why the so-called superlattice approach to creating such materials is receiving so much attention. In the superlattice approach, the functionality of a combined heterostructure depends on the interacting components and can be adjusted depending on the desired property. In the present paper, we present supercells of ferromagnetic thin films of Fe and Co deposited on ferroelectric and piezoelectric substrates of BaTiO<sub>3</sub> and SrTiO<sub>3</sub> that exhibit magnetism, ferroelectric polarization and piezoelectric effects. Within the structures under investigation, magnetic moments can be tuned by an external electric field via the ferroelectric dipoles. We investigate the effect of magnetoelectric coupling by means of ab initio spin-polarized and spin-orbit calculations. We study the structural, electronic and magnetic properties of heterostructures, and show that electrostriction can reduce the magnitude of the magnetization vector of a ferromagnet. This approach can become the basis for controlling the properties of one of the ferromagnetic layers of a superconducting spin valve, and thus the superconducting properties of the valve.

**Keywords:** magneto-electric coupling; DFT; heterostructure; reverse magnetostriction



**Citation:** Piyanzina, I.; Evseev, K.; Kamashev, A.; Mamin, R. Ab Initio Characterization of Magnetoelectric Coupling in Fe/BaTiO<sub>3</sub>, Fe/SrTiO<sub>3</sub>, Co/BaTiO<sub>3</sub> and Co/SrTiO<sub>3</sub> Heterostructures. *Magnetism* **2023**, *3*, 215–225. <https://doi.org/10.3390/magnetism3030017>

Academic Editor: Xavier Moya

Received: 16 May 2023

Revised: 9 June 2023

Accepted: 19 July 2023

Published: 31 July 2023



**Copyright:** © 2023 by the authors. Licensee MDPI, Basel, Switzerland. This article is an open access article distributed under the terms and conditions of the Creative Commons Attribution (CC BY) license (<https://creativecommons.org/licenses/by/4.0/>).

## 1. Introduction

In recent years, experimental and technological advances in the atomic layer-controlled growth of various multicomponent systems have allowed for the construction of various heterointerfaces composed of different materials [1]. The main advantage of such complex systems is their resulting functionality, which depends on the composition, defects, stress, etc. The development of the superlattice approach has allowed for the creation of materials with structures of which the properties could be tuned by an external influence [2]. For example, the addition of ferroelectric material as a component of a heterostructure might significantly extend the functionality required for conceptually new electronic devices. In particular, due to spontaneous polarization in the ferroelectric thin film, two-dimensional gas (2DEG) can occur at the interface. The electron mobility may also be enhanced by the external field via ferroelectric polarization [3–6]. Even more promising than manipulation of the electronic or magnetic state by an electric field is the implementation of the inverse magneto-electric effect, by which the magnitude of the magnetization and the direction of the magnetization can be changed by an electric field [7]. Ferromagnetic (FM)/ferroelectric (FE) oxide heterostructures are of particular interest due to their possible incorporation into modern multimode tunable spintronic devices. An extension of the functionality of existing devices, as well as a discovery of new devices, demands new materials that can provide

higher speed, smaller size and more efficient energy than traditional current-controlled schemes [8–11].

Ref. [12] showed that superflexible multiferroic heterostructures based on iron and classical ferroelectric (Fe/BaTiO<sub>3</sub>) demonstrate an ideal crystallinity and possibilities of epitaxial growth. In addition, such materials have some other outstanding properties, which positively affect the performance of devices based on them. In particular, they exhibit good multiferroic properties, a magnetoelectric (ME) coupling effect and reverse tunability of electronic and magnetic properties. The conjugate magnetic and electric fields can be used to control the respective order parameter with cross-coupling. For example, switching the ferromagnetic (FM) order using an electric field promises a significant impact on the development of next-generation devices. Magnetic tunnel junctions (MTJs) are of particular interest to the experimental and theoretical community due to their promising applications in magnetic random-access memory (MRAM). Multiferroic materials are also suitable for spin-filter purposes [13,14].

Another area of application of multiferroic heterostructures is the superconducting spin valve. It is known that the switching of superconductivity in a superconducting spin valve occurs with the help of an external magnetic field. Theoretical models of spin valves are based on the superconductor/ferromagnet proximity effect. The principle of operation of the spin valve is based on the fact that the value of the exchange field from two ferromagnetic layers acting on the Cooper pairs from the superconducting layer is greater in the case of parallel orientation of the magnetization of the ferromagnetic layers than in the case of an antiparallel orientation of the layers. This difference leads to a lower value of the transition temperature to the superconducting state in the case of parallel orientation of the magnetizations of the ferromagnet layer than in the case of an antiparallel orientation. The main condition for being able to control the superconducting current in the designs of a superconducting spin valve is  $\Delta T_c > \partial T_c$ , where  $\Delta T_c$  is the magnitude of the effect of the superconducting spin valve and  $\partial T_c$  is the width of the superconducting transition. At present, the control of a superconducting current under the action of an external magnetic field in the design of a superconducting spin valve has reached its maximum efficiency. To progress further, it is necessary to study new heterostructures with other switching capabilities. One such approach is the study of structures based on piezoelectric substrates. This offers the possibility of controlling the superconducting current in a superconducting spin valve using an electric field.

In this work, we present the results of a comparative study of film heterostructures based on ferromagnetic and ferroelectric materials. Superlattice structures based on Fe/BaTiO<sub>3</sub> (BTO), Fe/SrTiO<sub>3</sub> (STO), Co/BaTiO<sub>3</sub> and Co/SrTiO<sub>3</sub> were studied using density functional theory (DFT) calculations. The choice of components was motivated by the fact that Fe and BaTiO<sub>3</sub> are two “classical” ferroic materials with well-known bulk properties. In addition, fcc Fe and BaTiO<sub>3</sub> (Figure 1a,b) have similar cubic structures, which permits the experimental layer-by-layer epitaxial growth of Fe = BaTiO<sub>3</sub> multilayers without significant misfit dislocations, as well as simplifying the simulation of the heterostructures on a computer. Furthermore, since the Fe/BTO heterostructure has already been studied in depth [15–20], in this work, we present a comparison with heterostructures based on similar compounds, namely, ferromagnetic Co and quantum paraelectric SrTiO<sub>3</sub> (potential ferroelectric), in which the quantum fluctuations suppress the phase transition from the paraelectric to the ferroelectric state [21]. Duan et al. [16] showed that changing the direction of polarization could change the magnetization inside a ferromagnetic film. Thus, a change in direction of the magnetization could be used in devices for switching magnetization and superconductivity by an electric field in a superconducting spin valve. Here, we show that isotropic striction affects the magnitude of the magnetic moments. To study the striction effect, compression and tension were applied isotropically within the  $x$  and  $y$  axes.

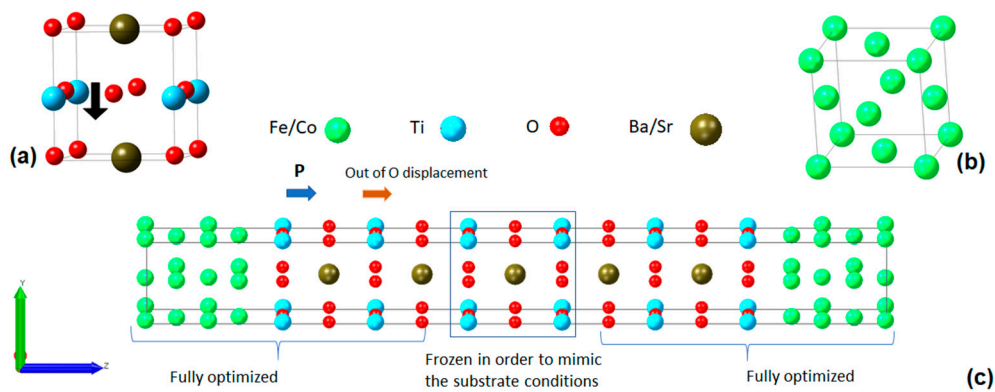


**Figure 1.** (a) The unit cells of BaTiO<sub>3</sub> at the tetragonal phase (SrTiO<sub>3</sub> has similar perovskite structure) and (b) fcc Fe(Co); and (c) the heterostructures Ba(Sr)TiO<sub>3</sub>/Fe(Co) used for simulations with arrows indicating the displacement of Ti from the center of oxygen octahedra and corresponding ferroelectric polarization in BTO.

## 2. Material and Method Details

Ab initio calculations were performed on the basis of the density functional theory [22]. The exchange and correlation effects were accounted for using the generalized gradient approximation (GGA) through the PBE functional (Perdew, Burke and Ernzerhoff parameterization) [23]. The Kohn–Sham equations [24] were solved using projectively extended wave potentials and wave functions [25]. All calculations were carried out using the VASP (Vienna ab initio Simulation Package) program [26] built into the MedeA computational software [27]. The cutoff of the plane wave was 400 eV, the convergence criterion for atomic relaxation was 0.02 eV/Å and the convergence condition for self-consistent calculations was the invariance in the total energy of the system, with an accuracy of  $10^{-5}$  eV. The Brillouin zones were separated using Monkhorst–Pack grids [28–30], including  $5 \times 5 \times 1$  k-points for Fe/BaTiO<sub>3</sub>, Fe/SrTiO<sub>3</sub>, Co/BaTiO<sub>3</sub> and Co/SrTiO<sub>3</sub> film heterostructures (Figure 1c), with a Gaussian smearing of 0.05 eV. To take into account strong correlations between the electrons of the *d*-shells, the calculations were performed within the GGA + *U* method using a simplified approach proposed by Dudarev et al. [31], which takes into account only the difference between the Coulomb screening parameter *U* and the Stoner exchange parameter *J* ( $U_{eff} = U - J$ ). In addition, a correct exchange is necessary for both the correct electronic and magnetic structure and correct geometry [32]. We applied additional local correlations  $U_{eff}$  equal to 4.4 eV and 4.6 eV for the Ti 3*d* and Fe 3*d* orbitals [33], respectively. To simplify the calculations, the following procedure was used: the geometry optimization was performed within the spin-polarized approach, whereas electronic and magnetic properties were extracted within the spin–orbit calculations [34].

In this work, the cells of heterostructures were modeled as superlattices (Figure 1c) with seven (or thirteen) atomic layers of Fe (or Co) alternating the slab of eleven atomic layers of BTO (or STO). To simulate the substrate conditions, the middle three atomic layers of BTO (STO) were “frozen” during the optimization procedure (their atomic positions were not changed).

## 3. Results and Discussions

It is well known that bulk Fe and Co are ferromagnetic metals. The calculations performed for the bulk components showed that the magnetic moments of Fe and Co ions in the bulk geometry are 2.99 and 1.72  $\mu_B$ , respectively. These values, together with the cell parameters, coincide well with previously published experimental values and theoretical predictions [10,26]. For our calculations, we used fcc cells of ferromagnetic materials (Figure 1b, note, that Co and Fe have the same structure). As for the BTO and STO chosen in this work, they have a perovskite cell with Ti surrounded by an oxygen octahedral (Figure 1a). The ferroelectric BTO in the tetragonal phase has a Ti–O displacement of 0.13 Å

(the displacement direction is shown by an arrow in Figure 1a), which corresponds to  $31 \mu\text{C}/\text{cm}^2$ , while in STO, there are no displacements in volume.

As was noted in the introduction, the structures of all four compounds are similar; however, the mismatch is relatively big, at up to 12% (Table 1), and causes a tensile appearance at the interface. The mismatch was calculated by  $(a_{\text{BTO}} - a_{\text{Fe}})/a_{\text{BTO}}$ , where  $a$  is a lattice parameter. To compose heterostructures, the components were brought into contact with an expansion of ferromagnetic slabs, but without any rotation. Alongside that, the BTO and STO were considered substrates, so the lattice parameters of the constructed heterostructures were kept frozen during the optimization procedure to the bulk values of the BTO and STO.

**Table 1.** Mismatch (in %) between the components of the constructed heterostructures.

	SrTiO <sub>3</sub>	BaTiO <sub>3</sub>
Co	9.4%	11.8%
Fe	6.5%	8.9%

Since there are four possible types of interfaces depending on the contact layers, we performed structural optimizations for all possible structures to find the most stable interface with the lowest energy. The following options are possible: a TiO<sub>2</sub> interface with O atoms over Fe/Co atoms (1) or Ti over Co atoms; (2) as well as a Ba(Sr)O interface with Ba(Sr) atoms; (3) and O over Co atoms and O in quadruple voids of the fcc Co(001) plane (4). Figure 1c shows the most stable interface configuration corresponding to the first type. This conclusion is consistent with the previous works [19,35]. Further discussion is presented for the most stable geometry.

### 3.1. Spin-Polarized Calculations: Structural and Magnetic Properties

As a result of optimization, the final structures undergo structural reconstructions and exhibit ferromagnetic properties. The resulting supercell is shown in Figure 1c. In order to characterize the structural distortions, we plot displacements of Ti atoms out of the oxygen planes depending on the layer in the perovskite slabs (BTO or STO). The results are summarized in Figure 2a. These rumpling inside the TiO<sub>2</sub> layers are associated with polarization. Similar plots were observed in [36], where the incensement of rumpling was observed close to the interfaces. More smooth curves would be observed with increased BTO(STO) slabs. It should be noted that the middle three layers were frozen in our computation scheme, and because of that, there are zero displacements. The other layers undergo complex distortions, with the highest out-of-plane shifts for interfacial atomic layers. The biggest magnitude corresponds to the BTO/Co heterostructure.

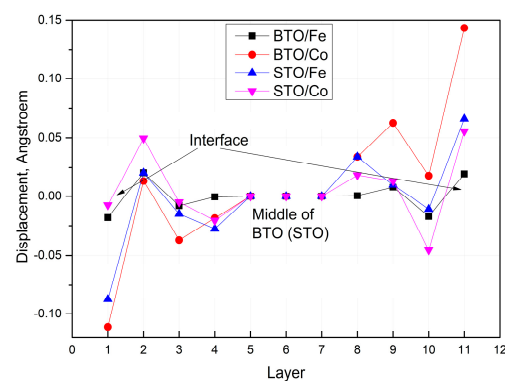


**Figure 2.** The displacement of Ti atoms out of oxygen planes in TiO<sub>2</sub> layers within the substrate (BTO or STO). The middle three atomic layers were frozen. Layers 1 and 11 correspond to the interfacial layers of the BTO (STO) in various heterostructures.

There is no doubt that the arising magnetism of the considered heterostructures is due to the presence of the ferromagnetic layers of iron or cobalt; however, the distribution of magnetization is different from the bulk. Indeed, Figure 3a shows the values of magnetic moments calculated per iron/cobalt ion of each layer of the ferromagnetic slab. As expected, we obtained an Fe slab with a slightly higher magnetization than the Co slab, since the bulk magnetic moments are different. Inside the ferromagnetic slab, magnetic moments are distributed uniformly, whereby a slight increase corresponds to the interfacial layers (layers 1 and 7). Inside the slab, it decays away from the interfaces and is practically constant for the BTO/Co interface, while in the BTO/Fe heterostructure, the values are oscillating near  $3.15 \mu_B$ . For BTO/Fe, the values of the magnetic moments at the interface are slightly higher than those in [12]. In addition, the magnitudes of the Ti moments were also summarized in Figure 3b. We found that only interfacial titanium atoms receive magnetic moments, and the magnitude of magnetization agrees well with the values published in [10] for the BTO/Fe case. The highest magnitudes of  $\sim 0.4\text{--}0.5 \mu_B$  correspond to the heterostructures with Fe. Alongside that, the Ti magnetic moments have directions opposite to that of the Fe moments which are toward the ferroelectric slab.

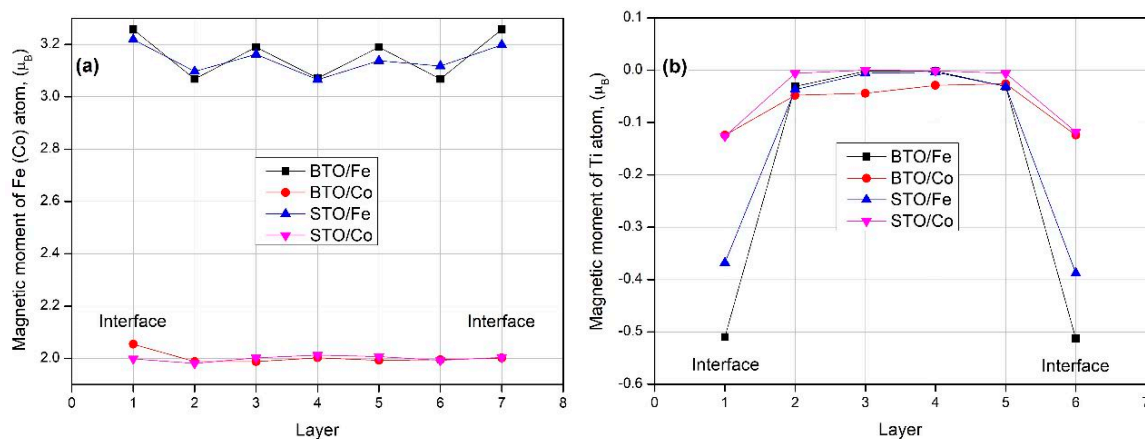


**Figure 3.** Average magnetic moments calculated within the spin-polarized approach for heterostructures with seven atomic layers of ferromagnet. (a) The magnetic moment values calculated per Fe/Co ion for different layers of the ferromagnetic film. (b) The magnetic moment values calculated per Ti ion for different layers of the BTO (STO). Layer 1 and layer 7 correspond to the interfacial layers within the ferromagnetic slab.

The last could be explained by the change in the bond length of Ti–Fe caused by ferroelectric displacements. According to Figure 1c, polarization causes the Ti atoms to move from the interface toward the center of the BTO(STO) slab, away from the interface. This causes the Fe–Ti bond length to become longer, and hence the overlap between the Fe  $3d$  and Ti  $3d$  orbitals becomes smaller. As can be seen from Figure 2, the biggest displacement was for BTO/Co, and the smallest for BTO/Fe, accounting for why we got the opposite dependence for Ti magnetization, with the biggest for BTO/Fe, and the smallest for BTO/Co and STO/Co. Thus, the ferroelectric instability reduces the induced magnetic moment on the Ti atoms.

Finally, the magnetization of the ferromagnetic cobalt film is uniformly distributed over the layers and is always about  $2 \mu_B$  per Co atom, which is slightly higher than the value in the bulk cobalt. In contrast to the case with iron, no rumpling was observed.

### 3.2. Spin–Orbit Calculations

In the considered heterostructures, we expect spin–orbit interactions to take place. A spin–orbit calculation enables examining the magnetic moment distribution over the different directions inside heterostructures. Indeed, as presented in Figure 4, the magnetization distribution is different from what was carried out for the spin-polarized calculations

(Figure 3a). The magnitude of the magnetic moments did not change, except for the BTO/Fe curve. However, the qualitative situation changed. The rumpling within the BTO/Fe and STO/Fe almost despaired, and the magnetization smoothly increases approaching the interfaces. Moreover, the magnitude of magnetic moments for Fe in BTO/Fe now agrees with values from [10]. Finally, we conclude that the magnetic moment is predominantly directed along the z-axis (in accordance with the cell demonstrated in Figure 1c). In Figure 3, other contributions from the  $xy$  plane were not added, since they are negligibly small all along the slab.

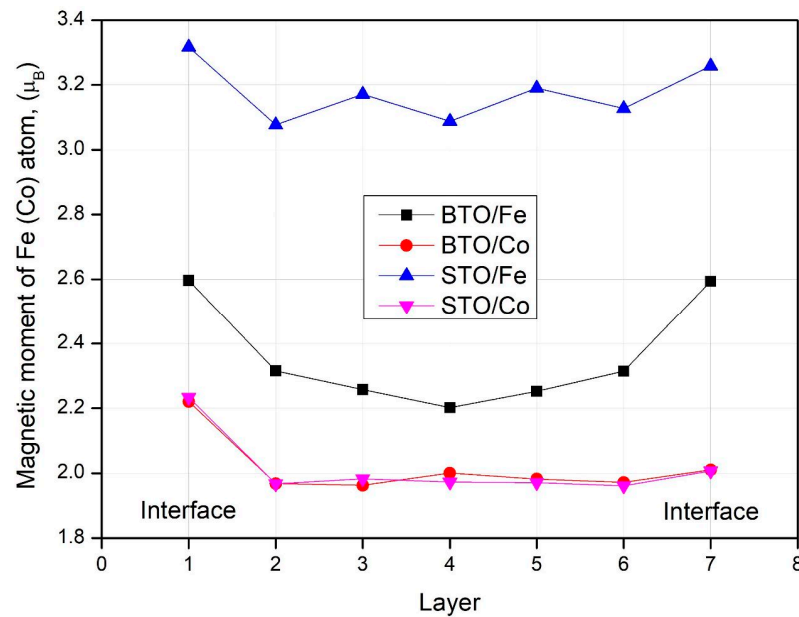


**Figure 4.** Average magnetic moments calculated taking into account the spin–orbit interaction. Magnetic moments were calculated per Fe (Co) ion in the ferromagnetic layers of the heterostructures. The results are shown for the  $z$  Cartesian direction only, whereas the magnetic moments in other directions are negligible (in accordance with Figure 1). Layer 1 and layer 7 correspond to the interface layers, whereas layer 4 is the middle layer of the ferromagnetic slab.

Experiments suggest that magnetization has an in-plane orientation. However, the thickness of experimental films is sufficiently larger. On the contrary, in the calculations, only small thicknesses are accessible due to the computation cost. Here, we deduced that the magnetization vector is directed perpendicular to the interface in the ferromagnetic slab up to 18 Å, which corresponds to 13 atomic layers of the ferromagnetic slab. A possible reason may be the following: the magnetization is directed along the  $z$ -axis in accordance with the so-called shape anisotropy, which leads to the appearance of an anisotropy axis perpendicular to the film plane. At the same time, for sufficiently thick films used in experiments, the demagnetizing factor is predominant, and the magnetization vector immediately chooses a more energetically favorable direction parallel to the surface and interface planes. We expect that for the sufficient thickness and additional striction applied in one direction ( $x$  or  $y$ ), the magnetization vector will choose a plane parallel to the interface.

### 3.3. Density of State Calculations

The nature of the induced magnetic moments at the interface can be understood from the partial local densities of states (DOS). Figures 5 and 6 show the spin-polarized atom-resolved densities of states for various atoms located in the interfacial layers of the considered heterostructures, namely, for the Ti  $3d$ , Fe/Co  $3d$  and O  $2p$  orbitals. The resulting plots indicate the presence of hybridizations between the above states, since an overlap on the energy scale takes place. For all plots,  $2p$  orbitals of oxygen atoms are located well below the Fermi energy and overlap with the Fe  $3d$  states. The maximum of DOS of Ti

$3d$  states for all heterostructures (Figures 5 and 6) is located approximately 3 eV above the Fermi energy and overlaps well with the Fe  $3d$  states. Hybridization between the  $3d$  orbitals of Fe (Co) and Ti creates a bond between the states that shifts down and peaks just below the Fermi level (seen for Fe and Co). Thus, the minor spin states of the Fe–Ti  $3d$  bond cause a charge redistribution between the major and minor spins, which leads to a greater occupation of the minor Ti spin states. This indicates the presence of an induced magnetic moment on the Ti atoms, directed antiparallel to the magnetic moment of Fe, where the states with the fundamental spin are (by definition) more occupied than the states with the minor spin. That conclusion agrees with the data for the magnetic moments shown in Figure 3a,b.

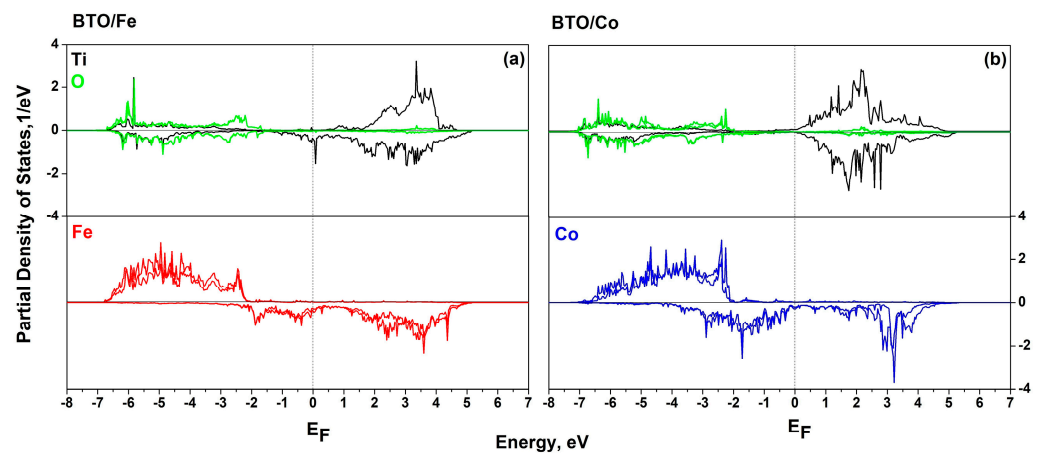


**Figure 5.** Atom-resolved density of states plots calculated for the BTO/Fe (a) and BTO/Co (b) heterostructures. Majority and minority spin DOSs are shown in the upper and lower panels, respectively. Zero at the energy scale corresponds to the Fermi level. Ti states are shown by the black curve, O by the green, Fe by the red and Co by the blue.

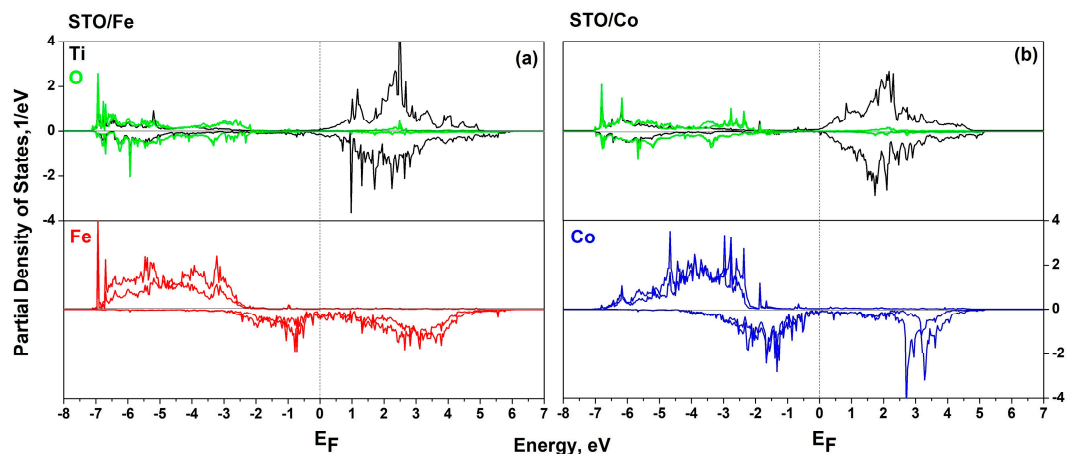


**Figure 6.** Density of states plots calculated for the STO/Fe (a) and STO/Co (b) heterostructures. Majority and minority spin DOSs are shown in the upper and lower panels, respectively. Zero at the energy scale corresponds to the Fermi level. Ti states are shown by the black curve, O by the green, Fe by the red and Co by the blue.

For the BTO/Co and STO/Co heterostructures, in addition to the above conclusions, the bond between Co  $3d$  and O  $2p$  (Figures 5b and 6b) is stronger than between Ti  $3d$  and Co  $3d$  orbitals. For this reason, in the case of cobalt, there is no dependence of the magnetization on the atomic layer, which is observed in heterostructures with iron.

In the case of STO/Fe DOS plots, a similar situation is observed:  $2p$  orbitals of oxygen atoms (Figure 6a) are located below the Fermi energy and do not have a good overlap with

the states of Fe (Co)  $3d$  and Ti  $3d$ . In the case of STO/Co, electronic interactions of the atoms located at the interface are characterized by a strong bonding between the  $3d$  orbitals of Co (Figure 6b) and the  $2p$  orbitals of O. The graph also shows that the bond between Co  $3d$  and O  $2p$  is much stronger than the overlap between Ti  $3d$  and Co  $3d$  orbitals.

### 3.4. Striction Calculations

The BTO/Fe heterostructure was chosen to study the effect of reverse magnetostriction. Starting from the value of the lattice parameter  $a = 4 \text{ \AA}$  ( $a = b$ ) within the spin-polarized calculations with a step of  $0.1 \text{ \AA}$ , the lattice was compressed in the  $xy$  plane and structural optimization for atomic positions was performed. The results for various compressions are summarized in Figure 7, demonstrating the distribution over ferromagnetic slabs. Since the calculations were carried out in the presence of additional stresses in the structure, this slightly affected the calculation results and we obtained jumps in some charts. However, the overall tendency of a slight decrease was observed: the average magnetic moment per ferromagnet atom changes from  $\sim 3.15 \mu_B$  for the initial structure to  $\sim 2.8 \mu_B$  for the structure with 15% compression. Additionally, we found that the difference between the interfacial and bulk Fe increases as the striction increases. In particular, structures with significant compression demonstrated the occurrence of maximum at the interfaces and in the middle of the ferromagnetic slab, while the minimum corresponded to the second layer from the interface.

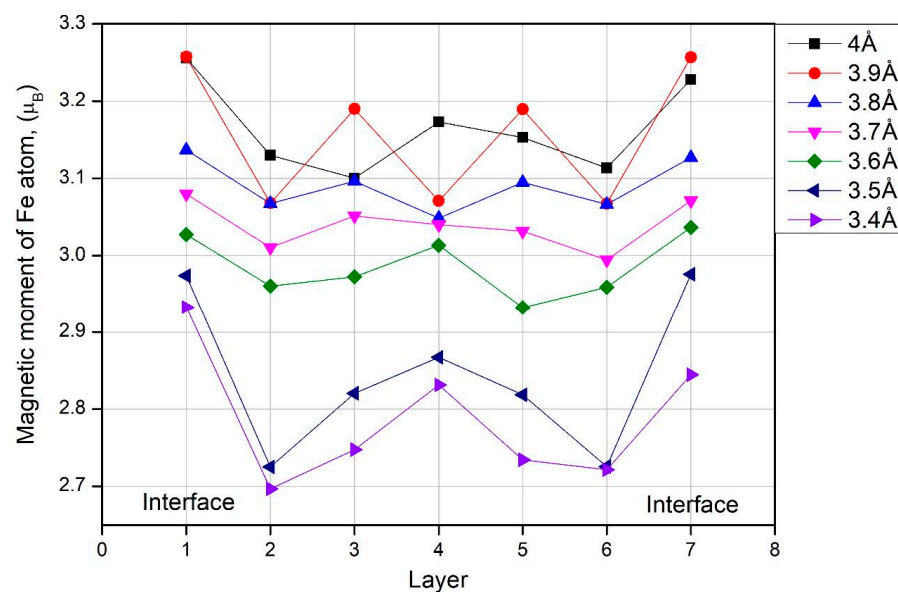


**Figure 7.** Magnetic moments of the Fe atoms calculated for the BTO/Fe heterostructure within the plane striction. Each curve corresponds to the in-plane  $a = b$  lattice parameters.

## 4. Discussion and Conclusions

The structural, electronic and magnetic properties of ferromagnet/ferroelectric heterostructures were studied for Fe/BaTiO<sub>3</sub>, Fe/SrTiO<sub>3</sub>, Co/BaTiO<sub>3</sub> and Co/SrTiO<sub>3</sub> model superlattice systems using the density functional theory approach. It was found that the structural properties of all considered heterointerfaces are similar: the structural optimization performed taking into account the magnetic nature of the materials led to the distortions associated with the movement of Ti and Ba(Sr) atoms from their bulk positions. The resulting magnitudes of out-of-oxygen plane displacements are the biggest at the interfacial layer due to the proximity of the ferromagnet. This is true for all investigated structures. On the contrary, the layer-dependent magnitude of displacement is different for all, and it depends both on the type of ferroelectric and ferromagnet used in the heterostructure. Taken together, these distortions lead to the appearance of polarization directed from the interface toward the ferroelectric substrate.

At the next stage, spin-polarized calculations revealed that the magnetic properties of heterostructures are also different for different ferromagnetic films used: while in the heterostructures with cobalt the magnetic moments are rather uniformly distributed over the thickness of the ferromagnet, the BTO/Fe and STO/Fe heterostructures have a rumpling inside the ferromagnetic layers. As expected, the values of magnetic moments are different, since the bulk values of Co and Fe magnetic moments differ as well. In addition, a slight increase at the interface was found. Oppositely directed magnetic moments appeared within the Ti interfacial atoms in ferroelectric slabs due to the ferroelectric polarization. The magnitude might be changed by reversed polarization, as well as by striction.

In order to investigate the spatial distribution of magnetic moments, spin-orbit calculations were applied. We revealed that the present geometry of a small thickness of the magnetization vector is directed along the  $z$ -axis due to the shape anisotropy. We expect that for a sufficient thickness, as well as with applied striction in one direction, the magnetic dipoles will choose a more energetically favorable direction parallel to the interface plane, consistent with experimental findings.

Finally, it was found that the applied voltage and, consequently, the striction in the plane parallel to the interface, change the magnetization distribution in the investigated BTO/Fe heterostructure. In particular, the values of magnetic moments decrease as the striction increases. Furthermore, the distribution within the slab changes: the slabs with the biggest compression demonstrate a maximum at the interface and a minimum at the second from the interface layer. We expect the same behavior for all similar structures.

The obtained results might be used in experimental studies on magnetization switching, as well as in studies on superconductivity switching in a superconducting spin valve.

**Author Contributions:** Conceptualization, I.P.; methodology, K.E.; software, K.E.; validation, R.M.; formal analysis, A.K.; investigation, I.P.; resources, I.P.; data curation, K.E.; writing—original draft preparation, I.P.; writing—review and editing, R.M. and A.K.; visualization, I.P.; supervision, R.M.; project administration, I.P.; funding acquisition, R.M. and A.K. All authors have read and agreed to the published version of the manuscript.

**Funding:** The reported study was funded by the Russian Scientific Foundation according to research project no. 21-72-10178 and the state task of the FRC KazSC RAS. Within the framework of the Russian Science Foundation grant no. 21-72-10178, a study on BTO/Fe and BTO/Co was carried out, whereas the heterostructures of STO/Fe and STO/Co were analyzed within the framework of the state task of the Federal Research Center of KazSC RAS.

**Institutional Review Board Statement:** Not applicable.

**Informed Consent Statement:** Not applicable.

**Data Availability Statement:** The data presented in this study are available on request from the corresponding author.

**Acknowledgments:** Computational resources were provided by the laboratory for computer design of new materials and machine learning of Kazan Federal University. All individuals have consented to the acknowledgement.

**Conflicts of Interest:** The authors declare no conflict of interest.

## References

1. Guo, W.; Posadas, A.B.; Demkov, A.A. Epitaxial integration of BaTiO<sub>3</sub> on Si for electro-optic applications. *J. Vac. Sci. Technol.* **2021**, *9*, 030804. [[CrossRef](#)]
2. Spaldin, N.A.; Ramesh, R. Advances in magnetoelectric multiferroics. *Nat. Mater.* **2019**, *18*, 203–212. [[CrossRef](#)] [[PubMed](#)]
3. Fredrickson, K.D.; Demkov, A.A. Switchable conductivity at the ferroelectric interface: Nonpolar oxides. *Phys. Rev.* **2015**, *91*, 115126. [[CrossRef](#)]

4. Niranjana, M.K.; Wang, Y.; Jaswal, S.S.; Tsybmal, E.Y. Prediction of a switchable two-dimensional electron gas at ferroelectric oxide interfaces. *Phys. Rev. Lett.* **2009**, *103*, 016804. [[CrossRef](#)] [[PubMed](#)]
5. Piyanzina, I.; Mamin, R. Toward the ferroelectric field-effect transistor on BaTiO<sub>3</sub>/LaMnO<sub>3</sub> heterostructure: DFT investigation. *J. Mater. Sci.* **2022**, *57*, 1–10. [[CrossRef](#)]
6. Liu, X.; Tsybmal, E.Y.; Rabe, K.M. Polarization-controlled modulation doping of a ferroelectric from first principles. *Phys. Rev.* **2018**, *97*, 094107. [[CrossRef](#)]
7. Weng, Y.; Niu, W.; Huang, X.; An, M.; Dong, S. Ferroelectric control of a spin-polarized two-dimensional electron gas. *Phys. Rev.* **2021**, *103*, 214101. [[CrossRef](#)]
8. Won, S.S.; Seo, H.; Kawahara, M.; Glinsek, S.; Lee, J.; Kim, Y.; Jeong, C.K.; Kingon, A.I.; Kim, S.H. Flexible vibrational energy harvesting devices using strain-engineered perovskite piezoelectric thin films. *Nano Energy* **2019**, *55*, 182–192. [[CrossRef](#)]
9. Yao, J.; Song, X.; Gao, X.; Tian, G.; Li, P.; Fan, H.; Huang, Z.; Yang, W.; Chen, D.; Fan, Z.; et al. Electrically driven reversible magnetic rotation in nanoscale multiferroic heterostructures. *ACS Nano* **2018**, *12*, 6767–6776. [[CrossRef](#)]
10. Hou, Y.; Wei, Y.; Yang, D.; Wang, K.; Ren, K.; Zhang, G. Enhancing the Curie Temperature in Cr<sub>2</sub>Ge<sub>2</sub>Te<sub>6</sub> via Charge Doping: A First-Principles Study. *Molecules* **2023**, *28*, 3893. [[CrossRef](#)]
11. Wang, K.; Ren, K.; Hou, Y.; Cheng, Y.; Zhang, G. Physical insights into enhancing magnetic stability of 2D magnets. *J. Appl. Phys.* **2023**, *133*, 11. [[CrossRef](#)]
12. Lu, N.; Zhang, P.; Zhang, Q.; Qiao, R.; He, Q.; Li, H.B.; Wang, Y.; Guo, J.; Zhang, D.; Duan, Z.; et al. Electric-field control of tri-state phase transformation with a selective dual-ion switch. *Nature* **2017**, *546*, 124–128. [[CrossRef](#)] [[PubMed](#)]
13. Borek, S.; Braun, J.; Ebert, H.; Minár, J. Multiferroic heterostructures for spin filter applications: An ab initio study. *Phys. Rev.* **2015**, *92*, 174408. [[CrossRef](#)]
14. Fechner, M.; Maznichenko, I.V.; Ostanin, S.; Ernst, A.; Henk, J.; Bruno, P.; Mertig, I. Magnetic phase transition in two-phase multiferroics predicted from first principles. *Phys. Rev.* **2008**, *78*, 212406. [[CrossRef](#)]
15. Leksin, P.V.; Garif'yanov, N.N.; Garifullin, I.A.; Schumann, J.; Vinzelberg, H.; Kataev, V.; Klingeler, R.; Schmidt, O.G.; Buchner, B. Full spin switch effect for the superconducting current in a superconductor/ferromagnet thin film heterostructure. *Appl. Phys. Lett.* **2010**, *97*, 102505. [[CrossRef](#)]
16. Duan, C.G.; Tsybmal, E.Y.; Jaswal, S.S. Predicted magnetoelectric effect in Fe/BaTiO<sub>3</sub> multilayers: Ferroelectric control of magnetism. *Phys. Rev. Lett.* **2006**, *97*, 047201. [[CrossRef](#)]
17. Zhao, Y.; Peng, R.; Guo, Y.; Liu, Z.; Dong, Y.; Zhao, S.; Li, Y.; Dong, G.; Hu, Y.; Zhang, J.; et al. Ultraflexible and malleable Fe/BaTiO<sub>3</sub> multiferroic Heterostructures for functional devices. *Adv. Funct. Mater.* **2021**, *31*, 2009376. [[CrossRef](#)]
18. Velez, J.P.; Duan, C.G.; Belashchenko, K.D.; Jaswal, S.S.; Tsybmal, E.Y. Effects of ferroelectricity and magnetism on electron and spin transport in Fe/BaTiO<sub>3</sub>/Fe multiferroic tunnel junctions. *J. Appl. Phys.* **2008**, *103*, 07A701. [[CrossRef](#)]
19. Duan, C.G.; Sahoo, S.; Srinivas, P.; Jaswal, S.S.; Tsybmal, E.Y.; Binek, C. Ferroelectric control of magnetism in BaTiO<sub>3</sub>/Fe heterostructures via interface strain coupling. *Phys. Rev.* **2007**, *76*, 092108. [[CrossRef](#)]
20. Cao, D.; Wang, F.; Jiang, Z.; Wu, T.; Jiao, Z.; Shu, H.; Cai, M.; Hu, W. Interfacial structure, ferroelectric stability, and magnetoelectric effect of magnetoelectric junction FeCo/BaTiO<sub>3</sub>/FeCo with alloy electrode. *J. Mater. Sci.* **2016**, *51*, 3297–3302. [[CrossRef](#)]
21. Müller, K.A.; Burkard, H. SrTiO<sub>3</sub>: An intrinsic quantum paraelectric below 4 K. *Phys. Rev.* **1979**, *19*, 3593. [[CrossRef](#)]
22. Kresse, G.; Furthmüller, J. Efficiency of ab-initio total energy calculations for metals and semiconductors using a plane-wave basis set. *Comput. Mater. Sci.* **1996**, *6*, 15–50. [[CrossRef](#)]
23. Perdew, J.P.; Burke, K.; Ernzerhof, M. Generalized gradient approximation made simple. *Phys. Rev. Lett.* **1996**, *77*, 3865. [[CrossRef](#)] [[PubMed](#)]
24. Kohn, W.; Sham, L.J. Self-consistent equations including exchange and correlation effects. *Phys. Rev.* **1965**, *140*, A1133. [[CrossRef](#)]
25. Blöchl, P.E. Projector augmented-wave method. *Phys. Rev.* **1994**, *50*, 17953. [[CrossRef](#)]
26. Kresse, G.; Furthmüller, J. Efficient iterative schemes for ab initio total-energy calculations using a plane-wave basis set. *Phys. Rev.* **1996**, *54*, 11169. [[CrossRef](#)]
27. Medea, version 3.7; Materials Design, Inc.: San Diego, CA, USA, 2023.
28. Monkhorst, H.J.; Pack, J.D. Special points for Brillouin-zone integrations. *Phys. Rev.* **1976**, *13*, 125188. [[CrossRef](#)]
29. Blöchl, P.E.; Jepsen, O.; Andersen, O.K. Improved tetrahedron method for Brillouin-zone integrations. *Phys. Rev.* **1994**, *49*, 16223. [[CrossRef](#)]
30. Methfessel, M.; Paxton, A.T. High-precision sampling for Brillouin-zone integration in metals. *Phys. Rev.* **1989**, *40*, 3616. [[CrossRef](#)]
31. Dudarev, S.L.; Botton, G.A.; Savrasov, S.Y.; Humphreys, C.J.; Sutton, A.P. Electron-energy-loss spectra and the structural stability of nickel oxide: An LSDA+U study. *Phys. Rev.* **1998**, *57*, 1505. [[CrossRef](#)]
32. Pham, A.; Assadi, M.H.N.; Yu, A.B.; Li, S. Critical role of Fock exchange in characterizing dopant geometry and magnetic interaction in magnetic semiconductors. *Phys. Rev.* **2014**, *89*, 155110. [[CrossRef](#)]
33. Calderon, C.E.; Plata, J.J.; Toher, C.; Oses, C.; Levy, O.; Fornani, M.; Natan, A.; Mehl, M.J.; Hart, G.; Nardelli, M.B.; et al. The AFLOW standard for high-throughput materials science calculations. *Comput. Mater. Sci.* **2015**, *108*, 233–238. [[CrossRef](#)]
34. Steiner, S.; Khmelevskiy, S.; Marsmann, M.; Kresse, G. Calculation of the magnetic anisotropy projected-augmented-wave methodology and the case study of disordered Fe<sub>1-x</sub>Co<sub>x</sub> alloys. *Phys. Rev.* **2016**, *93*, 224425. [[CrossRef](#)]

35. Oleinik, I.I.; Tsybal, E.Y.; Pettifor, D.G. Atomic and electronic structure of Co/SrTiO<sub>3</sub>/Co magnetic tunnel junctions. *Phys. Rev.* **2001**, *65*, 020401. [[CrossRef](#)]
36. Li, W.; Lee, J.; Demkov, A. Extrinsic magnetoelectric effect at the BaTiO<sub>3</sub>/Ni interface. *J. Appl. Phys.* **2022**, *131*, 054101. [[CrossRef](#)]

**Disclaimer/Publisher's Note:** The statements, opinions and data contained in all publications are solely those of the individual author(s) and contributor(s) and not of MDPI and/or the editor(s). MDPI and/or the editor(s) disclaim responsibility for any injury to people or property resulting from any ideas, methods, instructions or products referred to in the content.